CRYSTAL GROWTH & DESIGN

Article

pubs.acs.org/crystal

Tautomeric Polymorphism of 4-Hydroxynicotinic Acid

Sihui Long,[†] Mingtao Zhang,[‡] Panpan Zhou,[§] Faquan Yu,[†] Sean Parkin,[∥] and Tonglei Li*[,‡]

[†]Key Laboratory for Green Chemical Process of Ministry of Education, School of Chemical Engineering and Pharmacy, Wuhan Institute of Technology, Wuhan, Hubei 430073, China

[‡]Department of Industrial and Physical Pharmacy, Purdue University, West Lafayette, Indiana 47907, United States

[§]Department of Chemistry, Lanzhou University, Lanzhou, Gansu 730000, China

[∥]Department of Chemistry, University of Kentucky, Lexington, Kentucky 40506, United States

Supporting Information

ABSTRACT: 4-Hydroxynicotinic acid (4-HNA) was discovered to exist in the solid state as either 4-HNA or its tautomer 4-oxo-1,4-dihydropyridine-3-carboxylic acid (4-ODHPCA) in three polymorphs and two hydrates. Packing motifs differ as each of the three oxygen atoms acts as the hydrogen-bond acceptor, respectively, in the anhydrate forms, while in the hydrate forms, water molecules participate in hydrogen bonding with 4-HNA. Phase behaviors of the forms were characterized by differential scanning calorimetry (DSC), hot-stage microscopy (HSM), and thermogravimetric analysis (TGA). It was found that anhydrates I and II converted into III during heating; the two hydrate forms dehydrated at different temperatures and eventually transformed into anhydrate III, and sublimation of all five forms led to form III when the crystals were heated. Quantum mechanical calculations were performed providing further insight into the polymorphism.

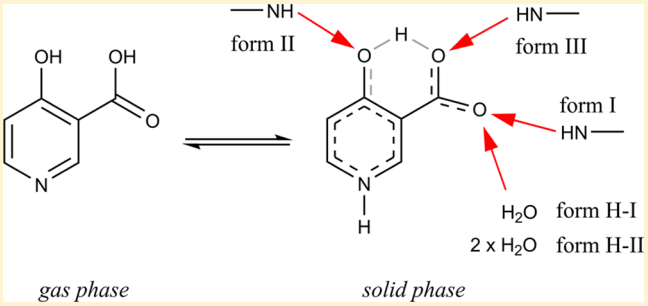

1. INTRODUCTION

Tautomerism is a well-known phenomenon in organic compounds with the ability of protons to shift from one atom to another. Enol/keto tautomers are the most frequently encountered,[1,2] while other tautomers such as sulfonimide−sulfonamide[3−5] are also observed. Hydroxypyridines (HPs) and hydroxynicotinic acids (HNAs) are prone to enol−ketonic tautomerization and are actively investigated. For example, 2-HP was shown to be present as either the enol or keto form in solution, depending on the polarity of the solvent.[6] Introduction of carboxylic acid to the 3 position of HP's pyridine ring leads to various HNAs, including 2-hydroxynicotinic acid (2-HNA), 4-HNA, 5-HNA, and 6-HNA. Detailed studies of the enol/keto tautomerization of HNAs in gas and solution phases were reported in the literature; for example, 2-HNA prefers the keto form while 4-HNA leans to the enol form.[7,8] Preference of one tautomeric form over another is obviously determined by the conformational energy, as well as by interaction with solvent molecules when in the solution phase. It is thus of a great interest to uncover how tautomerization of HNAs affects crystal packing of the molecules in the solid state. Our laboratory and others have systematically examined crystal structures of HNAs over the past few years.[8−10]

Studies of tautomeric polymorphism, particularly the keto−enol variety, date back at least 80 years.[2] In essence, polymorphism of such systems results from tautomerization of the molecules in question. Molecules that have been studied include triclabendazole,[11] barbituric acid,[12−15] omeprazole,[16] ranitidine,[17] sulfasalazine,[18] irbesarten,[19−21] 2-amino-3-hydroxy-6-phenylazopyridine,[22] and 2-(2,4-dinitrobenzyl)-3-methylpyridine.[23] Desmotropy is preferred by some researchers over the term tautomeric polymorphism.[24] Our studies of HNAs aimed to identify tautomers in the solid state and understand the influence by intermolecular interactions on the tautomeric preference. Four polymorphs were discovered for 2-HNA, and all four forms exist in the keto form, 2-oxo-1,2-dihydro-3-pyridinecarboxylic acid (2-ODHPCA), which is in agreement with the solution state study and gas phase calculations.[25] For 6-HNA, only one crystal structure was obtained and the molecule adopts the keto form.[26] Crystallization of 5-HNA failed to generate quality single crystals. Herein, we report crystal forms of 4-HNA and molecular identities in the solid state. In total, five crystal forms of 4-HNA were discovered, including three solvent-free polymorphs and two hydrates. Interestingly, both the enol and keto forms exist in the solid state, making the molecule a highly polymorphic system resulting from tautomerization. This is a rarity especially for a small and rigid molecule such as 4-HNA. Tautomerization of 4-HNA is illustrated in Scheme 1 along with its keto form, 4-ODHPCA. All possible tautomeric species are shown in Scheme 2. The molecule has shown some pharmacological

Received: November 20, 2015
Revised: March 28, 2016
Published: April 5, 2016

DOI: 10.1021/acs.cgd.5b01639
Cryst. Growth Des. 2016, 16, 2573−2580

Scheme 1. Enol-Keto Tautomerization of 4-Hydroxynicotinic Acid

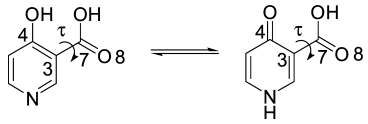

Scheme 2. Tautomeric Species of 4-Hydroxynicotinic Acid

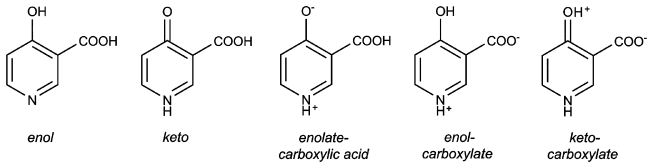

potential as it can be used to treat rheumatism and common cold associated symptoms such as nasal congestion and hoarseness.[27,28] In this report, detailed crystal structures and molecular packing are discussed, along with their thermal behaviors. Theoretical calculations were conducted to further interpret the tautomeric polymorphism.

2. EXPERIMENTAL SECTION

2.1. Materials. 4-HNA was synthesized by hydrolysis of 4-chloronicotinic acid (purchased from Alfa Aesar Co.),[25] purified by recrystallization from MeOH. The chemical purity of the compound was verified by solution NMR; no impurities were detected. It is also commercially available from a variety of vendors. All solvents were obtained from commercial sources and used as received.

2.2. Crystal Growth. The crystal growth method of slow evaporation or slow cooling was applied for polymorph screening of 4-HNA. For slow evaporation, the compound was dissolved in different solvents (aqueous and organic) forming saturated solutions at ambient temperature (~22 °C) (Table 1). The solutions were set for slow evaporation until single crystals were harvested. For example, 100 mg of 4-HNA was added to 10 mL of HPLC grade methanol. The mixture was stirred overnight, and the remaining solid was removed by pipet filtration. A vial containing clear solution was covered with perforated parafilm. Slow evaporation led to single crystals in about a week. For slow cooling, a saturated solution in a beaker covered by a cover glass was concentrated to one-third of the original volume by gently heating on a hot plate, and then the solution was cooled to room temperature with the heating turned off. All crystallization experiments were conducted in an unmodified atmosphere. Each experiment was repeated multiple times. Specifically, forms I, II, and III can be produced in methanol, acetone, and ethanol, respectively. And form III can also be obtained by sublimation from heating a solid sample. Hydrates I and II were both harvested from water. Note in methanol and water, crystals were grown in a noncontrollable fashion. The identity of the crystals was confirmed by powder X-ray diffraction and, when high quality single crystals were obtained, by single-crystal X-ray diffraction.

Table 1. Polymorph Screening of 4-HNA

solvent	growth condition	form
methanol	slow evaporation	II, III
methanol	slow evaporation	I
methanol	slow evaporation	I, II, III
methanol	slow cooling	I, II, III
methanol	slow cooling	II, III
acetone	slow evaporation	II
ethyl acetate	slow evaporation	II
isopropanol	slow evaporation	II
ethanol	slow evaporation	III
water	slow evaporation	H-I, H-II
water	slow evaporation	H-II
water	slow evaporation	H-I
water	slow cooling	H-I

2.3. Crystal Structure Determination. Crystal structures of the three anhydrates and two hydrates of 4-HNA were determined by single-crystal X-ray diffraction. For all five forms, data collection was carried out at 90 K on a Nonius kappaCCD diffractometer with Mo Kα radiation (λ = 0.71073 Å).[29] Cell refinement and data reduction were done using SCALEPACK and DENZO-SMN.[30] Structure solution and refinement were carried out using the SHELXS97 and SHELXL97 programs, respectively.[31−33] The hydrogen atoms involved in tautomerism in these structures were first located in difference electron density maps and subsequently refined freely with no ambiguity (for more clarification, see the Supporting Information).

Powder X-ray diffraction (PXRD) data for each sample were collected on a Rigaku X-ray diffractometer with Cu Kα radiation (40 kV, 40 mA; λ = 1.5406 Å) between 5.0 and 50.0° (2θ) at ambient temperatures. The finely ground sample was placed on a quartz plate in an aluminum holder.

2.4. Thermal Analyses. Phase behaviors of the solid forms were studied by differential scanning calorimetry (DSC), thermogravimetric analysis (TGA), and hot-stage microscopy (HSM). These experiments were performed on TA Instruments DSCQ20-1250, TGAQ50-0738, and INSTEC STC200, respectively. For DSC and TGA, Tzero pans and aluminum hermetic lids poked with holes were used at a heating rate of 10 °C/min. For HSM, a few crystals were placed on a glass slide, and a heating rate of 10 °C/min was used. The heating process was captured with a digital camera.

2.5. Computational Details. Single molecules of 4-HNA and 4-ODHPCA were optimized from various initial conformations at the B3LYP/6-311G++(d,p) level to identify the most stable conformations. The optimization was done by Gaussian09 (Gaussian, Inc., Wallingford, CT, USA) in gas phase or implicit solvent environments, including chloroform, dimethyl sulfoxide (DMSO), and water. The dielectric constants used in the calculation for these solvents were 4.71, 46.83, and 78.36, respectively. IEF (integral equation formalism) PCM (polarizable continuum model) was chosen as the solvation model. Frequency calculations were performed for all optimized structures to identify energy minima (zero imaginary frequency).

Intermolecular interactions and lattice energies of the anhydrate forms were calculated by first optimizing crystal structures. The optimization was conducted at the B3LYP/6-21G(d,p) level by Crystal14[34] where lattice parameters were kept the same as experimental values. Molecular pairs were then taken out of their respective crystal structures for the calculation of hydrogen-bonding strengths at the M06-2x/6-311g(2d,2p) level. The basis set superposition error (BSSE) was considered by the counterpoise method.[35] Moreover, the optimized crystal structures were calculated in order to derive the lattice energy, and for this purpose, dispersion energy contributions to lattice energy were considered by augmenting the DFT (density functional theory) results with damped, analytical energy models based on interatomic distances and predefined parameters.[36,37] BSSE was again handled by the counterpoise method. Energy convergence of the optimization and energy calculation was set to 10^{-7} hartree. Root-mean-square (RMS) values for calculation convergence were set to 0.0003 and 0.0012 au for energy gradient and atomic displacement, respectively. All calculations were conducted on a Linux cluster.

3. RESULTS AND DISCUSSION

3.1. Crystal Structures. Three anhydrates (I, II, and III) and two hydrates (H-I and H-II) of 4-HNA were discovered (Figure 1). Form I crystals were obtained as colorless blocks from methanol, form II crystals were grown as colorless rods from acetone, ethyl acetate, and isopropanol, and form III crystals were harvested as colorless prisms from ethanol. Structure determination by single-crystal X-ray diffraction

DOI: 10.1021/acs.cgd.5b01639
Cryst. Growth Des. 2016, 16, 2573−2580

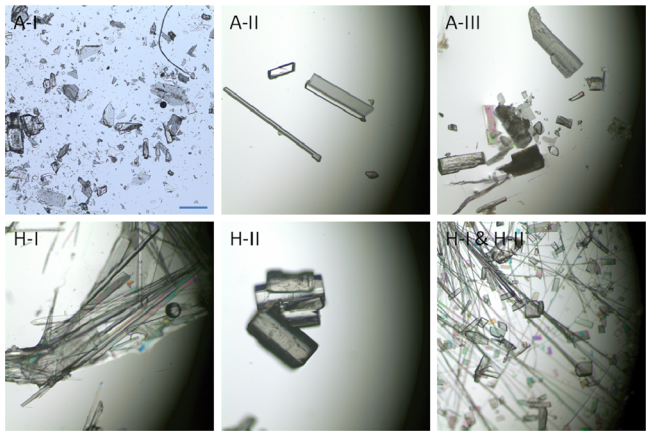

Figure 1. Crystals of the three anhydrates and two hydrates of 4-HNA. Scale bar, 0.2 mm.

found form I to be orthorhombic, space group $Pna2_1$ (Z = 4); form II to be monoclinic, space group $P2_1/c$ (Z = 4); and form III to be monoclinic, space group Cc (Z = 8). Hydrate I is orthorhombic, space group $P2_12_12$ (Z = 4), and hydrate II is monoclinic, space group $P2_1/c$ (Z = 4). Crystallographic data of the forms are listed in Table 2; for complete CIF files, see CCDC Nos. 1443388, 1443390, 1443392−1443393, and 1443396. Careful examination of the crystallographically independent molecules in each of the asymmetric units indicates they are conformationally similar, as suggested by the torsion angle between the carboxylic acid and the aromatic ring defined by O8C7C3C4 (ca. 174.5° in form I, −176.9° in form II, −176.4° in IIIa, 178.5° in IIIb, 179.4° in H-I, and 179.5° in H-II). A superposition of all six conformations in the polymorphs clearly indicates the conformational similarity (Figure 2). In the crystals of forms I, II, and H-I, the molecules take the keto form and the carboxylic acid group forms an *anti*

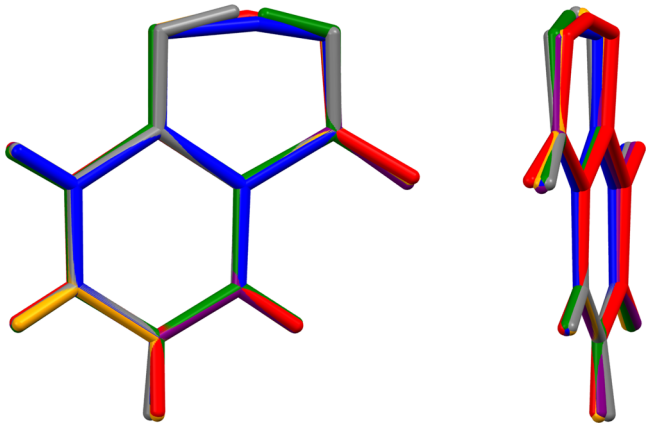

Figure 2. Superposition of six conformations in the asymmetric units of forms I, II, and III and H-I and H-II (I, red; II, green; IIIa, gray; IIIb, orange; H-I, blue; and H-II, purple).

configuration; in the crystals of forms III and H-II, the molecules adopt the enol form wherein the carboxylic acid proton is transferred to the pyridine N (i.e., enol-carboxylate in Scheme 2). In particular, due to the lack of centrosymmetry in form III, the crystal is polar.

In the anhydrate form I, the asymmetric unit consists of one molecule (Z' = 1). The molecule has a planar conformation, and the *anti* configuration of carboxylic acid precludes the possibility of forming acid−acid dimer motifs. Instead, the hydroxyl group of the acid forms an intramolecular hydrogen bond with the adjacent carbonyl O, with the distance and angle

Table 2. Crystallographic Data of Three Polymorphs and Two Hydrates of 4-HNA

	I	II	III	H-I	H-II
formula	$C_6H_5NO_3$	$C_6H_5NO_3$	$C_6H_5NO_3$	$C_6H_5NO_3.0.5H_2O$	$C_6H_5NO_3.H_2O$
fw	139.11	139.11	139.11	148.12	157.13
cryst size (mm)	0.20 × 0.17 × 0.10	0.30 × 0.20 × 0.10	0.20 × 0.20 × 0.02	0.25 × 0.20 × 0.10	0.22 × 0.18 × 0.10
cryst syst	orthorhombic	monoclinic	monoclinic	orthorhombic	monoclinic
space group	$Pna2_1$	$P2_1/c$	Cc	$P2_12_12$	$P2_1/c$
a/Å	13.4233(1)	3.71980(1)	3.6124 (1)	7.2840(2)	7.8418(3)
b/Å	3.8097(5)	14.5367(5)	22.8112 (7)	23.5200(3)	12.6104(6)
c/Å	11.6150(5)	10.6250 (4)	13.5495 (5)	3.6450(12)	7.2017(3)
α/deg	90	90	90	90	90
β/deg	90	93.3280 (15)	89.8980 (16)	90	113.9211(19)
γ/deg	90	90	90	90	90
Z, Z'	4, 1	4, 1	8, 2	4,1	4,1
V/Å^3	593.98(8)	573.56(3)	1116.52(6)	624.5(2)	650.99(5)
D_{cal}/(g·cm^{-3})	1.556	1.611	1.655	1.575	1.603
T/K	90(2)	90(2)	90.0(2)	90(2)	90(2)
abs coeff/mm^{-1}	0.127	0.132	0.136	0.132	0.137
F(000)	288	288	576	308	328
θ range/deg	3.04−27.40	2.38−27.46	1.50−27.49	1.73−27.45	2.84−27.49
limiting indices	$-16 \le h \le 17$	$-4 \le h \le 4$	$-4 \le h \le 4$	$-9 \le h \le 9$	$-10 \le h \le 10$
	$-4 \le k \le 4$	$-18 \le k \le 18$	$-28 \le k \le 28$	$-29 \le k \le 30$	$-16 \le k \le 16$
	$-14 \le l \le 15$	$-13 \le l \le 13$	$-17 \le l \le 17$	$-4 \le l \le 4$	$-9 \le l \le 9$
completeness to 2θ/%	100.0	99.9	97.3	100	99.9
unique reflecns	838	1367	1320	912	1573
R_1 [$I > 2\sigma(I)$]	3.58	5.52	4.01	5.11	4.30
R_{w2} (all data)	0.0928	0.1401	0.0989	0.1315	0.1168

DOI: 10.1021/acs.cgd.5b01639
Cryst. Growth Des. 2016, 16, 2573−2580

being 2.426 Å, and 156.34°, respectively. The carbonyl O of the carboxylic acid group forms a hydrogen bond with the secondary amino group NH, with the corresponding hydrogen-bonding parameters being 2.797 Å and 172.21°. These molecules form one-dimensional chains (Figure 3). Interestingly, the direction of the chains is the same, being along the *c* axis. The crystal is thus polar, although the space group is achiral.

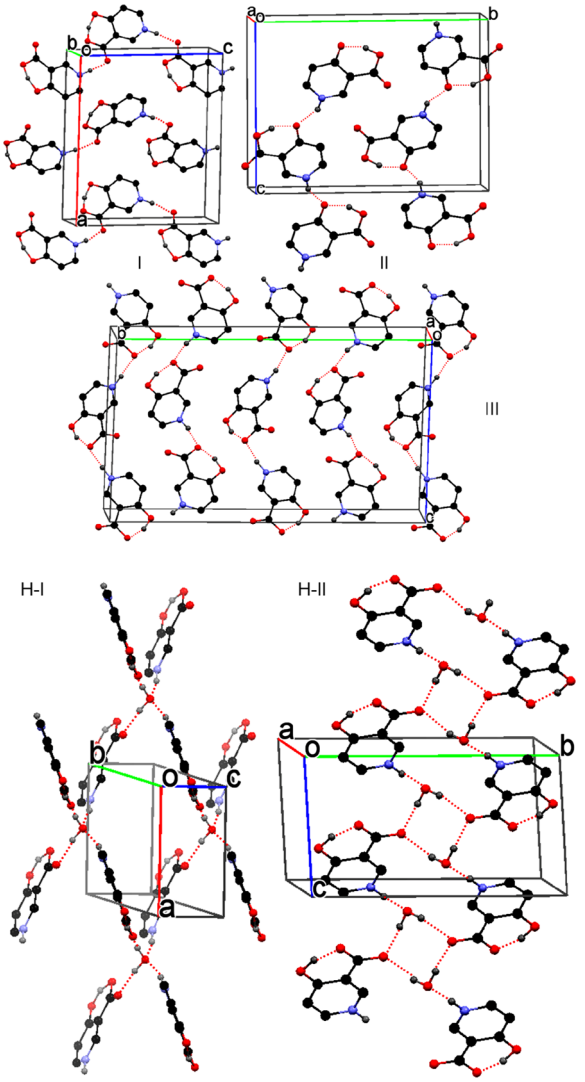

Figure 3. Crystal packing of anhydrates I, II, and III and hydrates I and II (for clarity, hydrogens not involved in hydrogen bonding are omitted).

Similar to form I, the anhydrate form II has one molecule in the asymmetric unit, which is nearly flat and in the *anti* configuration. The intramolecular hydrogen bonding between the OH of the carboxylic acid and the nearby O from the carbonyl has slightly different parameters, 2.518 Å and 158.23°. The intermolecular hydrogen bonding in this case, however, is between the exo O of the ring carbonyl and the secondary NH, with hydrogen-bonding parameters 2.730 Å and 152.66°. Essentially, this O acts as a bifurcated hydrogen-bond acceptor, leaving the other carbonyl O not involved in any hydrogen bonding. The crystal structure is based on one-dimensional chains propagating along the *b* axis with alternant hydrogen-bonding directions (Figure 3), thereby rendering the crystal apolar. This anhydrate form was also reported by Santos et al. although data were collected at 293 K in the latter case.[8] They show negligible difference in the unit cell parameters obviously due to the temperature variation during data collection.

The anhydrate III form crystallizes with two molecules (A and B) in the asymmetric unit ($Z' = 2$). Unlike anhydrates I and II, the molecules become zwitterionic with the carboxylic acid proton no longer associated with the O. The molecules are in the enol form. An intramolecular hydrogen bond is formed, similar to that of anhydrate I or II except for the position of the proton. The intramolecular hydrogen bond has identical parameters of 2.457 Å and 150.02° in molecules A and B. An intermolecular hydrogen bond is formed between adjacent molecules of the same conformation with slightly different parameters, 2.777 Å and 163.55° for A conformers and 2.776 Å and 167.71° for B. The one-dimensional hydrogen-bonded chains propagate along the *c* axis with alternating directions (Figure 3). Interestingly, the acceptor for the intermolecular hydrogen bond is from the deprotonated carboxyl, which is different from either I or II.

The three anhydrous polymorphs of 4-HNA, therefore, result not from conformation differences because the molecules have similar conformations, but from the different participants in the intermolecular hydrogen bonds, particularly dissimilar hydrogen-bond acceptors due to both the tautomerization and the proton transfer. As illustrated in the abstract graphic, the chief difference among the polymorphs stems from the three oxygen atoms of the molecule acting respectively as hydrogen-bonding acceptors in the crystal structures. In form I, the carbonyl O on the carboxylic acid forms a hydrogen bond with the NH from an adjacent molecule; in form II, the carbonyl O on the ring participates in the hydrogen bonding. The molecules in the two forms are nearly identical conformationally, and the intramolecular hydrogen bonds bear similar configurations. The only major variance is the bond angle of the intermolecular hydrogen bond (172.21° in form I and 152.66° in form II). Yet, form II is more compacted as indicated by its higher density (1.611 g·cm^{-3} in II vs 1.556 g·cm^{-3} in I). Form III appears drastically different from form I or II because not only is the molecule no longer in the keto form but also the proton has been transferred intramolecularly. The exo O on the ring is no longer a hydrogen-bond acceptor but a donor. One carboxylic acid O becomes a bifurcated hydrogen acceptor, forming the intramolecular hydrogen bond with enol OH and intermolecular hydrogen bond with NH. The intermolecular hydrogen bond shows the bond length similar to that of form I or II, but the bond angle is different from either. Among all three forms, it has the highest density at 1.655 g·cm^{-3}.

Hydrate I crystallized in the Sohnecke space group $P2_12_12$ with one 4-HNA molecule and one water molecule in the asymmetric unit. The 4-HNA molecule has a planar conformation with the carboxylic acid being *anti*. An intramolecular hydrogen bond is formed between the carboxylic acid OH and the adjacent carbonyl O (2.44 Å and 156.7°). In addition, each 4-HNA molecule participates in two intermolecular hydrogen bonds with water molecules (Figure 3). The hydrogen bonding between the 4-HNA NH and O of water has parameters 2.79 Å and 161.4°. The hydrogen bond between the OH of water and the carbonyl O of the carboxylic acid has parameters of 2.69 Å and 172.6°. Each water molecule is involved in four hydrogen bonds (two donors and two acceptors). The structure, thermal stability, and dehydration

DOI: 10.1021/acs.cgd.5b01639
Cryst. Growth Des. 2016, 16, 2573−2580

kinetics/mechanism of this hemihydrate have been reported.[9,10] The two structures have similar unit cell parameters with the previously known one showing a slightly higher cell volume since its diffraction data were collected at 296 K.

Hydrate II also consists of one 4-HNA molecule and one water molecule in the asymmetric unit of space group $P2_1/c$. The 4-HNA molecule shows a near flat conformation. Unlike H-I but similar to form III, proton transfer takes place and 4-HNA is zwitterionic. The carboxylic acid H shifts to the nearby exo O of the carbonyl and the molecule is in the enol form. A similar intramolecular hydrogen bond to that in form III exists with 2.48 Å and 148.6° of the hydrogen-bonding distance and angle, respectively. In addition, each 4-HNA molecule participates in three intermolecular hydrogen bonds with water molecules. The one between NH and O from water has hydrogen-bond parameters of 2.68 Å and 173.8°. The other two, between O of carboxylic acid and OH from two water molecules, have different strengths: the stronger one having parameters of 2.74 Å and 177.1° and the weaker one of 2.83 Å and 166.6°. In contrast to H-I, each water molecule only partakes in three hydrogen bonds, twice as donors and once as acceptor. Two water and two 4-HNA form a rectangular hydrogen-bonding motif of R_4^2 (8). The rectangle fuses with another large ring of R_4^4 (16) hydrogen-bonding motif. The collective construct leads to a staircase-like packing pattern perpendicular to the (1 0 1) face (Figure 3).

Keto−enol tautomerization as a base for polymorphism was investigated more than 80 years ago when Weygand studied the four modifications of acetyldibenzoylmethane.[38] Since then, there have been few well-defined cases of keto−enol tautomeric polymorphism. Our newly reported polymorphic system of 2-HNA can merely be considered as polymorphism of a tautomer. Yet, 4-HNA seems to be strikingly different from 2-HNA because both tautomers crystallized in the solid state. The molecule in form I is the keto tautomer, indicated by the bond length of 1.287 Å of C4−O10 and the proton associated with N1. Similar results can be found in form II with the bond length of 1.285 Å of C═O. For form III, the molecule adopts the enol form with bond lengths of 1.315 and 1.308 Å for the enol C−OH of the two conformers, respectively. The proton on the carboxylic acid is transferred to the pyridine N. For the two hydrate forms, H-I is of the keto form with C═O bond length of 1.294 Å while H-II is of the enol form with C−OH bond distance 1.323 Å. In H-II, the carboxyl is deprotonated, similar to form III. The results seem to suggest that the enol form is associated with the deprotonation of the carboxyl group in the solid state.

3.2. Thermal Properties. DSC was conducted to investigate the thermal properties of the five forms, shown in Figure 4. Form I shows multiple DSC peaks, whose onset temperatures are 67.5, 176.4, 227.0, and 255.6 °C. It seems that at around 68 °C (inset, Figure 4), form I undergoes a phase transition to become an intermediate phase, and the intermediate phase further converts into likely form II at around 176 °C (inset, Figure 4), which then transforms into form III at about 227 °C. Form II has two endothermic DSC peaks. The first one, with the onset temperature of 231.1 °C, appears to be a solid-to-solid phase transition to form III, and then the second one at 256.8 °C corresponds to melting of the new form. Form III shows one melting peak at an onset temperature of 259.8 °C. Hydrate I has three DSC events, dehydration at onset 65.1 °C, phase transition likely to form III at 240.1 °C, and melting at 260.9 °C. Similar to H-I, H-II shows

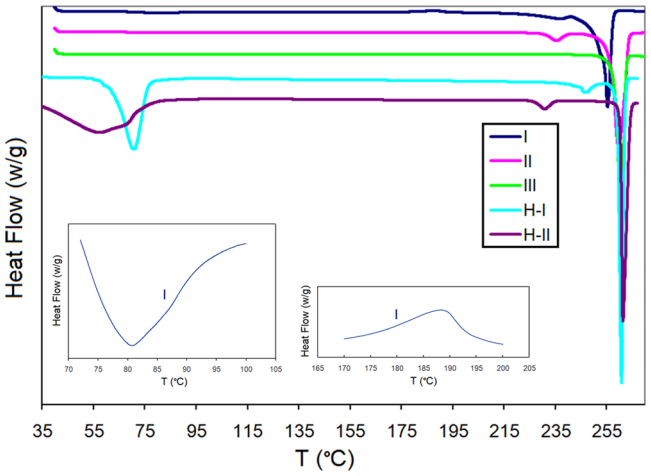

Figure 4. DSC thermograms of 4-HNA anhydrates and hydrates. Insets are of the form I.

three thermal events, dehydration at 32.0 °C, phase transition at 227.2 °C, and melting at 260.1 °C. The dehydration of hydrate forms was confirmed by TGA (see Supporting Information).

The phase behaviors were further studied under a hot-stage microscope. A solid-to-solid phase transition from form II single crystals to form III was captured (Figure 5). In addition, transformation to form III due to sublimation of either form I or II was observed. For example, when crystals of form II were heated to about 210 °C and held at that temperature for several hours, new crystals appeared on the cover glass gradually (Figure 6), which were identified as form III by single-crystal X-ray diffraction. Form III crystals also sublimed when heated on the hot-stage, but the resulting new crystals were still of form III. Given the fact that the 4-HNA molecules adopt a different tautomeric form in form I or II (i.e., keto) from that in form III (i.e., enol-carboxylate), it is reasonable to argue that the molecule undergoes tautomerization in the gas phase prior to crystallization, likely due to the enol form being more energetically favored in the gas phase than keto (as seen by our Computational Results). This is also supported by results in ref 8. Arguably, when the enol form crystallizes into form III, it would be of great interest to investigate whether the deprotonation process occurs simultaneously with the tautomerization or during the crystallization process. A similar sublimation-assisted tautomerization was reported for 2-thiobarbituric acid, in which the enol form II converts into the keto through sublimation.[13]

Figure 7 shows powder X-ray diffraction patterns of forms I, II, and III collected at room temperature, along with simulated patterns calculated from the single-crystal structures determined at 90 K. The similarity of each form between the experimental and simulated patterns indicates the thermodynamic stability at room temperature. The comparison also suggests that each batch of crystallization product was most likely of one polymorph, not a mixture of multiple polymorphs.

3.3. Computational Results. Conformational energies were calculated for single molecules of either enol or keto form in vacuum (gas phase) or implicit solvent environments. The results show that the enol form is preferred in the gas phase by a free energy difference of −8.2 kJ/mol, compared with the keto form. However, when the environment is polarizing, the keto form is stabilized and preferred over enol by free energy

DOI: 10.1021/acs.cgd.5b01639
Cryst. Growth Des. 2016, 16, 2573−2580

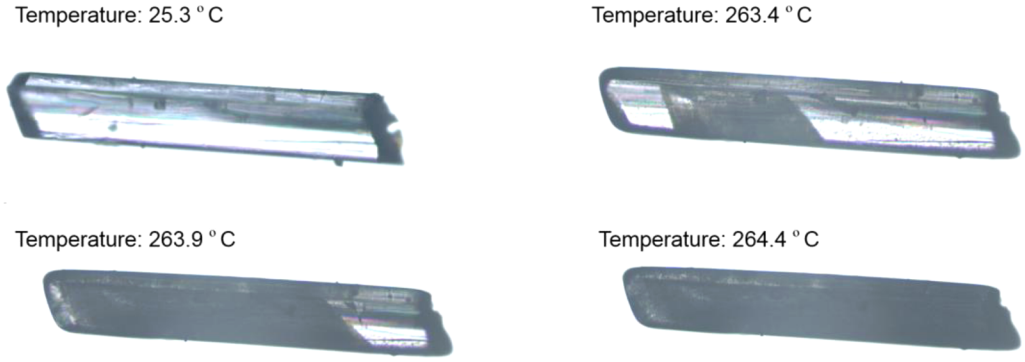

Figure 5. Solid-to-solid phase transition from form II to form III observed under a hot-stage microscope.

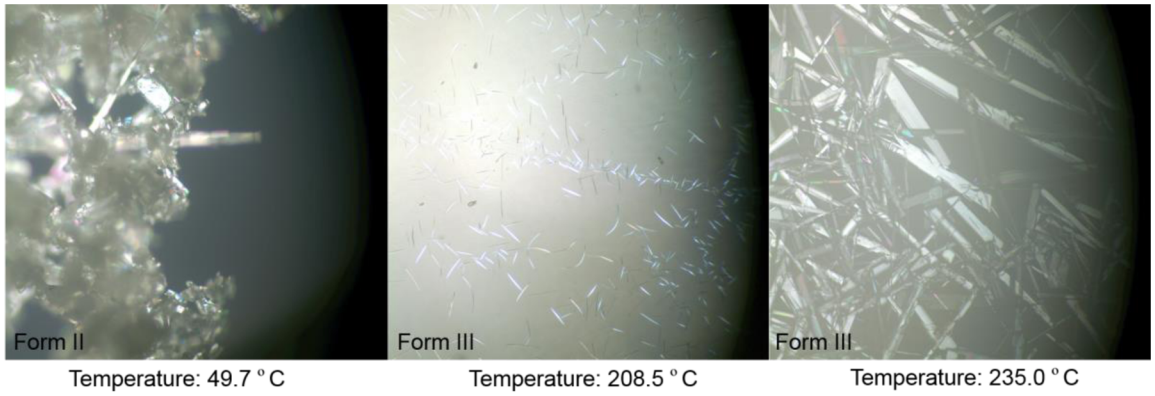

Figure 6. Sublimation-assisted phase transition from form II to form III.

differences of −16.4, −26.6, and −27.1 kJ/mol in continuous solvent models of chloroform, DMSO, and water, respectively. Interestingly, zwitterionic forms of enol and keto forms (Scheme 2) were not found to be stable during the calculation in either vacuum or an implicit solvent environment. Furthermore, when the molecule forms carboxyl−carboxyl hydrogen-bonded dimers, the keto form is always preferred over enol in vacuum (by −20.1 kJ/mol) or in a solvent model (by −7.2, −3.0, and −2.8 kJ/mol in chloroform, DMSO, and water, respectively).

Combined with the experimental results of form selection in different solvents (Table 1), the calculation indicates that preference of the keto form results from the polarity of the solvent, as well as intermolecular hydrogen bonding that forms in the solid state.

Intermolecular hydrogen-bonding strengths and lattice energies of the anhydrate forms were calculated. Hydrogen-bonded chains are formed in forms I, II, and III. Potential energies of each hydrogen bond are −65.3, −46.1, −81.2, and −95.2 kJ/mol for these chains in forms I, II, and III ($Z' = 2$), respectively. For comparison, the total potential energy of two hydrogen bonds in a carboxyl−carboxyl dimer (in the keto form) is −77.8 kJ/mol. The results suggest that the dimer motif is not energetically favored and pyridine N needs to be involved in the intermolecular hydrogen bonding in the solid state. Furthermore, the hydrogen bonding becomes more stabilized when the molecule adopts the enol form but requires deprotonation of the carboxyl group. The lattice energies calculated are −117.9, −121.8, and −105.4 kJ/mol for forms I, II, and III, respectively, indicating the stability order to be II > I > III with form II being the most stable. This is contradictory to the stability order based on the calculated densities which suggest III > II > I. And it also disagrees with the thermal study results since both forms I and II convert into form III. Yet, the lattice energy calculation compares total energy values of the three polymorphic structures against the energy of the same, most stable molecular conformation in vacuum, which is the enol form. If the comparison is made against the energy of the individual conformation found in each crystal, the respective packing energies of forms I, II, and III are −72.3, −61.7, and −103.7 kJ/mol. This illustrates that the total intermolecular interactions in form III are the strongest, in good agreement with form III being the most densely packed.

4. CONCLUSIONS

Three anhydrates and two hydrates of 4-HNA were obtained by crystallization from solution. The crystal structures demonstrate tautomeric polymorphism with the molecule either in the keto form as a neutral molecule (anhydrate forms I and II) or zwitterion (H-I), or in the enol form (forms III and H-I) which involves proton transfer from carboxyl to pyridine N. The molecule prefers the keto form in a polarized environment, but the enol form can form stronger intermolecular hydrogen bonding (with the carboxyl deprotonated). Carboxyl−carboxyl hydrogen-bonding dimer is not observed in the solid state, and pyridine N is always involved in the intermolecular hydrogen bonds. The polymorphism of the anhydrate forms may also be viewed as a result from the three O atoms acting as respective hydrogen-bonding acceptors. Thermal behaviors indicate that the molecule undergoes tautomerization in gas or solid phase from the keto to enol when crystals of forms I or II sublime and condense or transfer to form III. However, deprotonation of the enol form seems to be a prerequisite to accompany the tautomerization during the self-assembly process of molecules.

DOI: 10.1021/acs.cgd.5b01639
Cryst. Growth Des. 2016, 16, 2573−2580

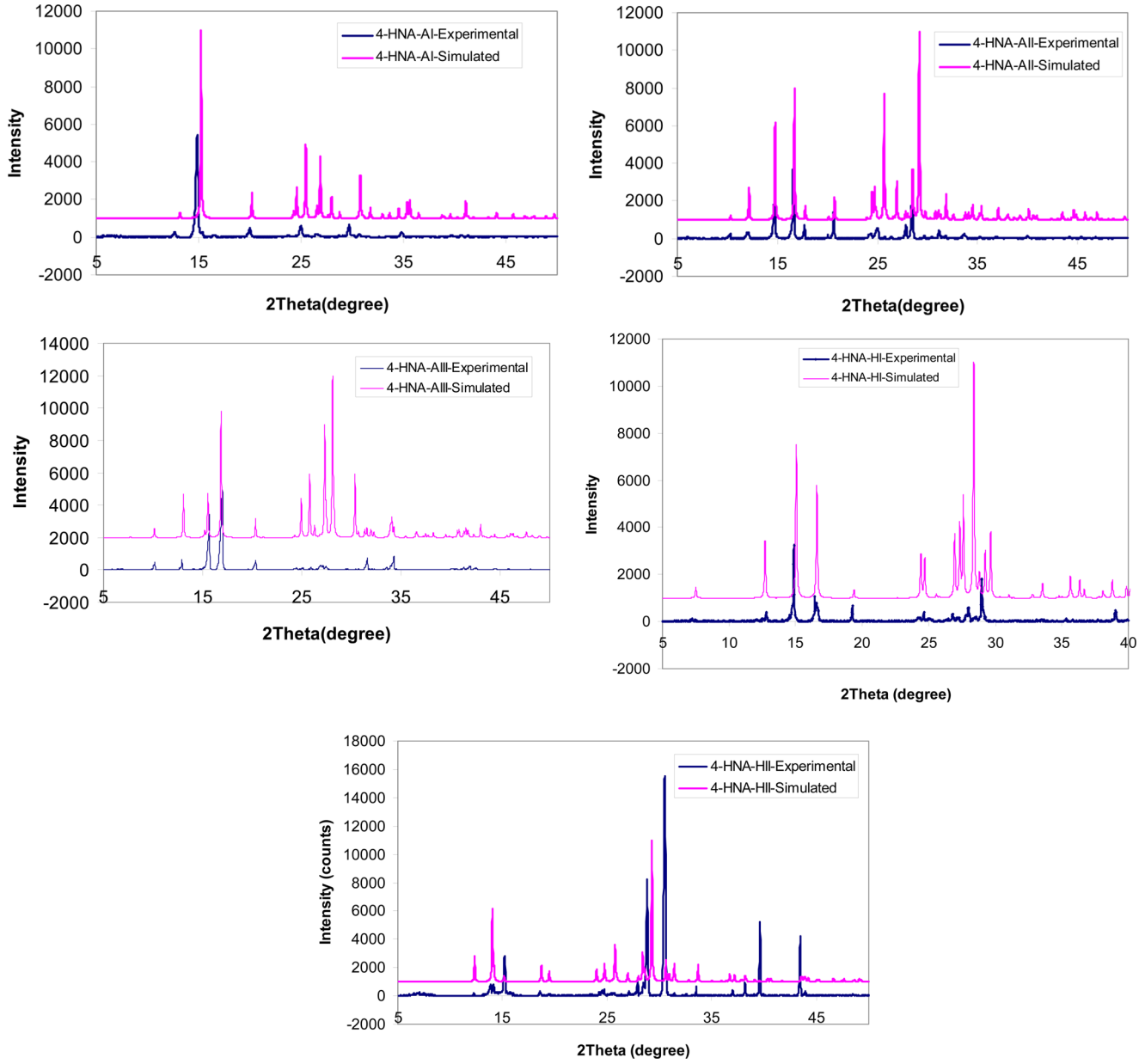

Figure 7. Experimental and simulated powder X-ray diffraction patterns of 4-HNA anhydrates (AI, AII, and AIII) and hydrates (HI and HII).

■ ASSOCIATED CONTENT

Supporting Information

The Supporting Information is available free of charge on the ACS Publications website at DOI: 10.1021/acs.cgd.5b01639.

Additional experimental results (PDF)

Accession Codes

CCDC 1443388, 1443390, 1443392−1443393, and 1443396 contain the supplementary crystallographic data for this paper. These data can be obtained free of charge via www.ccdc.cam.ac.uk/data_request/cif, or by emailing data_request@ccdc.cam.ac.uk, or by contacting The Cambridge Crystallographic Data Centre, 12, Union Road, Cambridge CB2 1EZ, UK; fax: +44 1223 336033.

■ AUTHOR INFORMATION

Corresponding Author

*Phone: (765) 494-1451. E-mail:tonglei@purdue.edu.

Notes

The authors declare no competing financial interest.

■ ACKNOWLEDGMENTS

S.L. thanks the Natural Science Foundation of Hubei Province for financial support (Grant No. 2014CFB787). P.Z. acknowledges the financial support by the National Natural Science Foundation of China (Grant No. 21403097) and the Fundamental Research Funds for the Central Universities (Grant No. lzujbky-2014-182). T.L. is grateful to NSF for supporting the work (Grant No. DMR1006364) and to the Allen Chao Endowment.

■ REFERENCES

(1) Dawson, H. M. *J. Chem. Soc., Trans.* **1913**, *103*, 1308.
(2) Grinard, V.; Blanchon, H. *Roczniki Chemii* **1929**, *9*, 547.
(3) Thomas, S. P.; Nagarajan, K.; Row, T. N. G. *Chem. Commun.* **2012**, *48*, 10559.

DOI: 10.1021/acs.cgd.5b01639
Cryst. Growth Des. 2016, 16, 2573−2580

(4) Thomas, S. P.; Shashiprabha, K.; Vinutha, K. R.; Nayak, S. P.; Nagarajan, K.; Row, T. N. G. *Cryst. Growth Des.* **2014**, *14*, 3758−3766.
(5) Lill, S. O. N.; Broo, A. *Cryst. Growth Des.* **2014**, *14*, 3704−3710.
(6) Bridges, J. W.; Davies, D. S.; Williams, R. T. *Biochem. J.* **1966**, *98*, 451−468.
(7) Dogra, S. K. *J. Mol. Struct.* **2005**, *737*, 189.
(8) Santos, R. C.; Figueira, R. M. B. B. M.; Piedade, M. F. M.; Diogo, H. P.; Minas da Piedade, M. E. *J. Phys. Chem. B* **2009**, *113*, 14291−14309.
(9) Matias, E. P.; Bernardes, C. E. S.; Piedade, M. F. M.; Minas da Piedade, M. E. *Cryst. Growth Des.* **2011**, *11*, 2803−2810.
(10) Joseph, A.; Bernardes, C. E. S.; Viana, A. S.; Piedade, M. F. M.; Minas da Piedade, M. E. M. *Cryst. Growth Des.* **2015**, *15*, 3511−3524.
(11) Tothadi, S.; Bhogala, B. R.; Gorantla, A. R.; Thakur, T. S.; Jetti, R. K. R.; Desiraju, G. R. *Chem. - Asian J.* **2012**, *7*, 330.
(12) Chierotti, M. R.; Gobetto, R.; Pellegrino, L.; Milone, L.; Venturello, P. *Cryst. Growth Des.* **2008**, *8*, 1454.
(13) Chierotti, M. R.; Ferrero, L.; Garino, N.; Gobetto, R.; Pellegrino, L.; Braga, D.; Grepioni, F.; Maini, L. *Chem. - Eur. J.* **2010**, *16*, 4347.
(14) Schmidt, M. U.; Bruning, J.; Glinnermann, J.; Hutzler, M. W.; Morschel, P.; Ivashevskaya, S. N.; van de Streek, J.; Braga, D.; Maini, L.; Chierotti, M. R.; Gobetto, R. *Angew. Chem.* **2011**, *123*, 8070−8072.
(15) Schimidt, M. U.; et al. *Angew. Chem., Int. Ed.* **2011**, *50*, 7924−7926.
(16) Bhatt, P. M.; Desiraju, G. R. *Chem. Commun.* **2007**, 2057.
(17) Mirmehrabi, M.; Rohani, R.; Murthy, K. S. K.; Radatus, B. *J. Cryst. Growth* **2004**, *260*, 517.
(18) Blake, A. J.; Lin, X.; Schroder, M.; Wilson, C.; Yuan, R. X. *Acta Crystallogr., Sect. C: Cryst. Struct. Commun.* **2004**, *60*, o226.
(19) Bauer, M.; Harris, R. K.; Rao, R. C.; Apperley, D. C.; Rodger, C. A. *J. Chem. Soc., Perkin Trans. 2* **1998**, *2*, 475.
(20) Bocskei, Z.; Simon, K.; Rao, R.; Caron, A.; Rodger, C. A.; Bauer, M. *Acta Crystallogr., Sect. C: Cryst. Struct. Commun.* **1998**, *54*, 808−810.
(21) Garcia, M. A.; Lopez, C.; Claramunt, R. M.; Kenz, A.; Pierrot, M.; Elguero, J. *Helv. Chim. Acta* **2002**, *85*, 2763−2776.
(22) Desiraju, G. R. *J. Chem. Soc., Perkin Trans. 2* **1983**, 1025.
(23) Schmidt, A.; Kababya, S.; Appel, M.; Khatib, S.; Botoshansky, M.; Eichen, Y. *J. Am. Chem. Soc.* **1999**, *121*, 11291.
(24) Elguero, J. *Cryst. Growth Des.* **2011**, *11*, 4731.
(25) Long, S.; Zhou, P.; Theiss, K. L.; Siegler, M. A.; Li, T. *CrystEngComm* **2015**, *17*, 5195.
(26) Gupta, S.; Long, S.; Li, T. *Acta Crystallogr., Sect. E: Struct. Rep. Online* **2007**, *63*, o2784.
(27) Hardy, J. D.; Wolff, H. G.; Goodell, H. *J. Clin. Invest.* **1940**, *19*, 649.
(28) Tendeloo, H. J. C.; Broekman, F. W.; Stsiemelink, J. J. U.K. Patent GB1362698, 1974.
(29) *Collect*; Nonius BV: Delft, the Netherlands, 2002.
(30) Otwinowski, Z.; Minor, W. In *Methods in Enzymology: Macromolecular Crystallography*, Part A; Abelson, J. N., Simon, M. I., Carter, C. W., Jr., Sweet, R. M., Eds.; Academic Press: New York, 1997; Vol. *276*, p 307.
(31) Sheldrick, G. M. Siemens Analytical X-ray Instruments: Madison, WI, USA, 1995.
(32) Sheldrick, G. M. *SHELXL97 and SHELXS97*; University of Gottingen: Gottingen, Germany, 1997.
(33) Sheldrick, G. M. *Acta Crystallogr., Sect. A: Found. Crystallogr.* **2008**, *64*, 112−122.
(34) Dovesi, R.; Orlando, R.; Erba, A.; Zicovich-Wilson, C. M.; Civalleri, B.; Casassa, S.; Maschio, L.; Ferrabone, M.; De La Pierre, M.; D'Arco, P.; Noel, Y.; Causa, M.; Rerat, M.; Kirtman, B. *Int. J. Quantum Chem.* **2014**, *114*, 1287.
(35) Boys, S. F.; Bernardi, F. *Mol. Phys.* **1970**, *19*, 553.
(36) Feng, S.; Li, T. *J. Chem. Theory Comput.* **2006**, *2*, 149.
(37) Li, T.; Feng, S. *Pharm. Res.* **2006**, *23*, 2326.
(38) Weygand, C. *Z. Anorg. Allg. Chem.* **1932**, *205*, 414.

DOI: 10.1021/acs.cgd.5b01639
Cryst. Growth Des. 2016, 16, 2573−2580